Electrodeposition of cuprous oxide on a porous Cu framework for an improved photoelectrochemical performance

Mario Kurniawan, Michael Stich, Mayra Marimon, Magali Camargo, Ralf Peipmann, Thomas Hannappel, and Andreas Bund

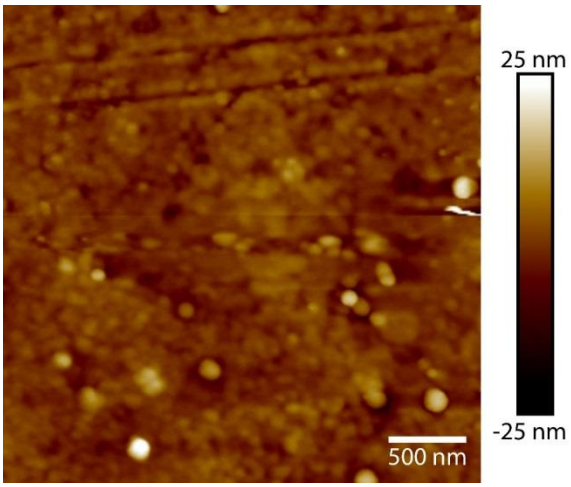

Fig. S1 Height topography of the electropolished flat Cu substrate with a root-mean-squared roughness, Rq, of ~3 nm.

The atomic force microscopy (AFM) measurement was carried out using the Dimension Icon AFM (Bruker) device equipped with a silicon nitride probe which has a resonant frequency of 70 kHz and a spring constant of 0.4 N m^{-1} (Scanasyst-air) from Bruker to provide information regarding the morphology and surface roughness. The measurement was done with PeakForce tapping mode which uses an operating frequency (1 kHz) well below the probe resonant frequency to obtain high-resolution images. The roughness value, Rq, was extracted using the NanoScope Analysis software from Bruker. The electropolished flat Cu substrate in Fig. S1 has a roughness value, Rq, of ~3 nm which shows that the surface is smooth.

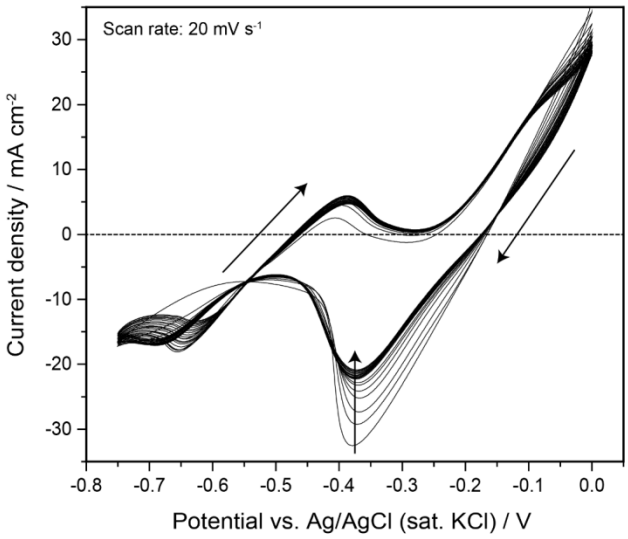

Fig. S2 Cyclic voltammogram of electrodeposition process of Cu_2O films on reinforced porous Cu substrate (at -1.5 A cm^{-2}, 60 s – reinforced for 120 min deposition time) in Cu citrate electrolyte at pH 12.3 recorded with a scan rate of 20 mV s^{-1} and 20 loop cycles. The arrow which points upward indicates the movement of the cathodic peak with the increasing cycle numbers.

The cyclic voltammetry analysis was done to investigate the reduction potential of Cu_2O on the reinforced porous Cu substrate (Fig. S2) which was near -0.4 V vs. Ag/AgCl (sat. KCl). It can be seen that there is a significant decrease in the current density near the scanned potential of -0.4 V vs. Ag/AgCl (sat. KCl) especially from the first cycle to the seventh cycle. The reaction seems to be saturated after the eighth cycle which indicates a slower deposition rate of the Cu_2O films.

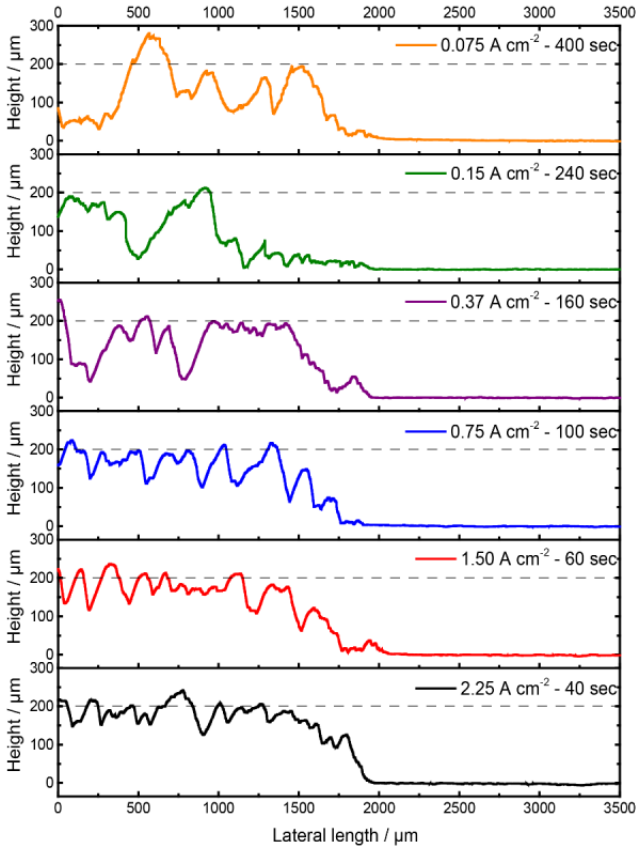

Fig. S3 Thickness comparison of the dendritic porous Cu structures electrodeposited with different current densities and durations using a profilometer.

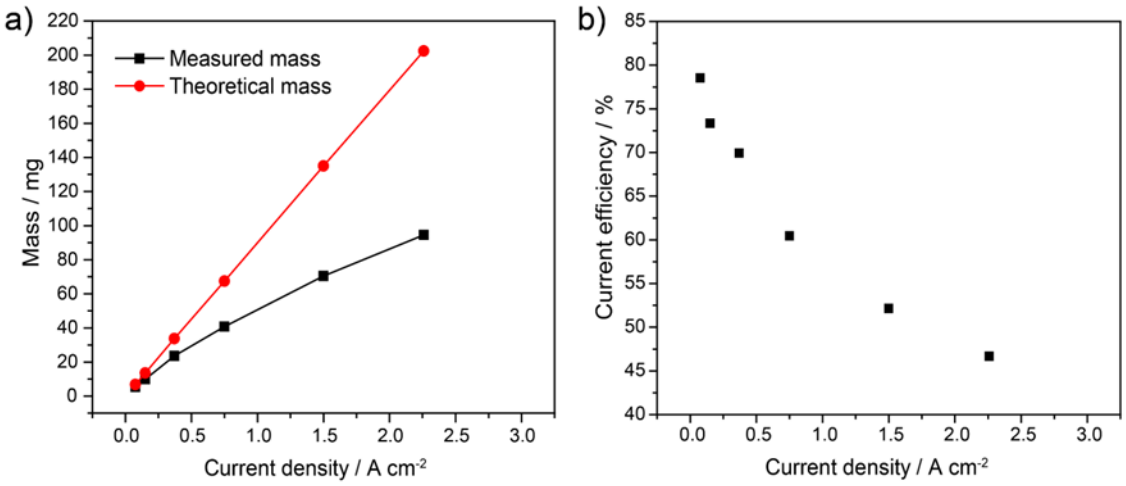

Fig. S4 Influence of applied current density on the change of a) mass and b) current efficiency for electrodeposited Cu on flat Cu substrate.

The theoretical mass as shown in Fig. S4a was derived according to Faraday's law of electrolysis (Equation (S1))

$$m = \frac{M \cdot Q}{n \cdot F} \tag{S1}$$

Where m is the calculated mass in grams (g), Q is the total charge which is measured in Coulombs (C), M is the molar mass of the substance (g mol^{-1}), F is the Faraday constant which is 96485 C mol^{-1} and n is the number of electrons per ion. The current efficiency was calculated based on the value of the measured mass of the Cu that was deposited on the flat Cu substrate against the theoretical mass. As the applied current density increases the current efficiency of the Cu deposition decreases significantly. It is likely due to the hydrogen evolution reaction that is occurring in parallel during the Cu electrodeposition process.

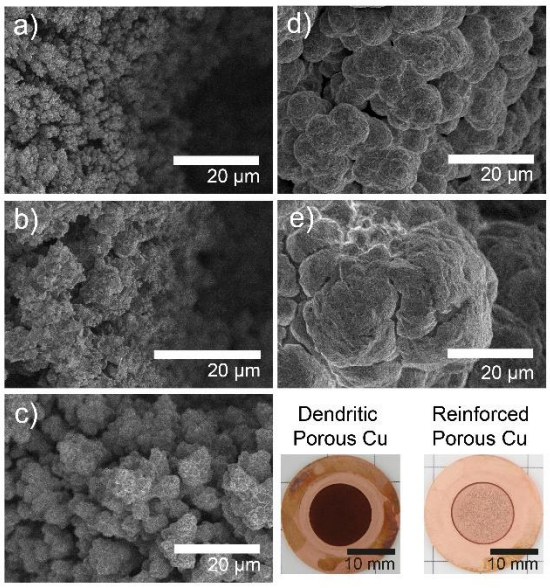

Fig. S5 SEM images of reinforcement process with second electrodeposition of Cu on dendritic porous Cu with a) no reinforcement, b) 5 min, c) 30 min, d) 60 min and e) 120 min reinforcement time.

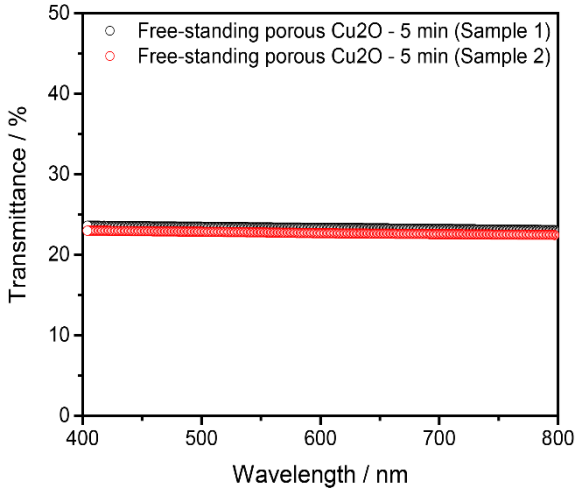

Fig. S6 Transmission spectra of free-standing porous Cu_2O electrodes which were electrodeposited at -1.5 A cm^{-2} in an acidic Cu bath for 60 sec, then reinforced with a second Cu electrodeposition at -20 mA cm^{-2} for 120 min and lastly potentiostatic Cu_2O deposition in an alkaline bath at -0.4 V vs. Ag/AgCl (sat. KCl) for 5 min.

The UV-Vis transmission spectroscopy was carried out using Cary 5000 UV-VIS-NIR spectrophotometer (Varian Inc) with a spectral range from 400 to 800 nm. At different wavelengths, the spectral is constant and no visible peaks can be observed (Fig. S6).

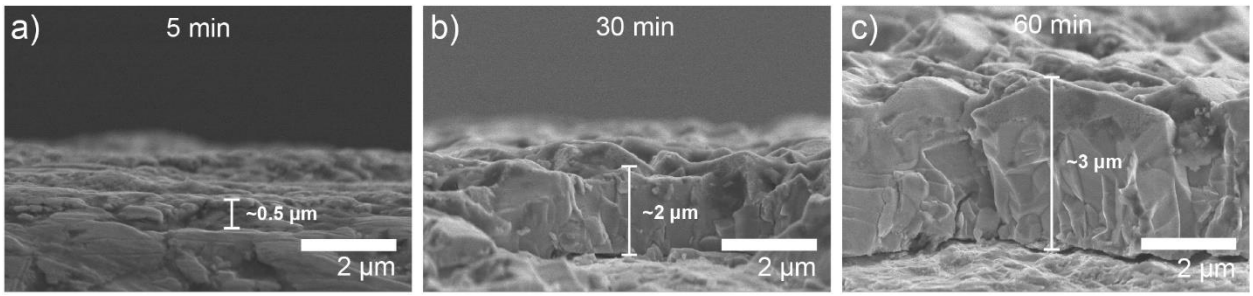

Fig. S7 Cross-sectional images of the Cu_2O film electrodeposited on flat Cu substrates at -0.4 V vs. Ag/AgCl (sat. KCl) in the alkaline copper bath for a) 5 min, b) 30 min and c) 60 min deposition time.

The thickness of the Cu_2O layer deposited at different durations is estimated from the SEM images in Fig. S7. The layer thickness increases from ~500 nm to 3 µm for the Cu_2O samples of 5 min to 60 min deposition time.

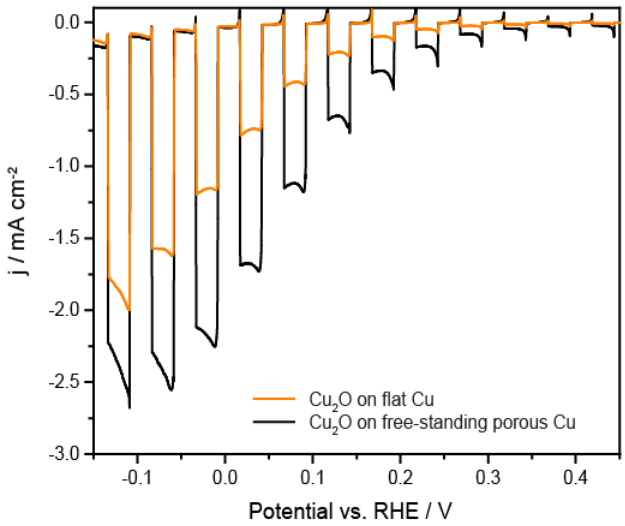

Fig. S8 Linear sweep voltammogram of Cu_2O film deposited on flat Cu substrate and free-standing porous Cu framework in 0.5 M Na_2SO_4 (pH 5.9) under chopped solar illumination of 100 mW cm^{-2}.

The linear sweep voltammogram in Fig. S8 shows a distinct comparison of the photoelectrochemical water splitting performance between the Cu_2O film deposited on a flat Cu and a free-standing porous Cu framework. The current densities at the potential of 0 V vs RHE increase about 80 % for the free-standing porous Cu_2O framework. The high surface area provided by the inner pore walls has improved the PEC performance significantly.

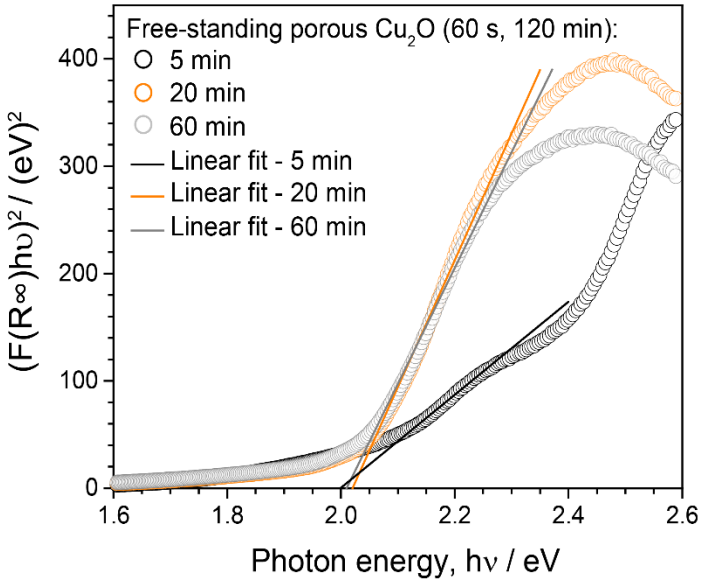

Fig. S9 Estimation of the bandgap using a Tauc plot obtained from Kubelka Munk function and the UV-Vis diffuse reflectance spectra of the Cu_2O film deposited on free-standing porous Cu frameworks with different deposition times.

The diffuse reflectance spectrum of the samples was obtained using Cary 5000 UV-Vis-NIR spectrophotometer (Varian Inc) with a spectral range from 400 to 800 nm. Tauc plot was established using the Kubelka-Munk function and the diffuse reflectance spectra as was represented in Fig. S9. Linear Tauc equation was used to fit the slope of the curve and the bandgap was estimated from the intersection of the linear fit where the y-axis is equal to zero which reveals a nearly identical value at ~2 eV for all the deposited samples.

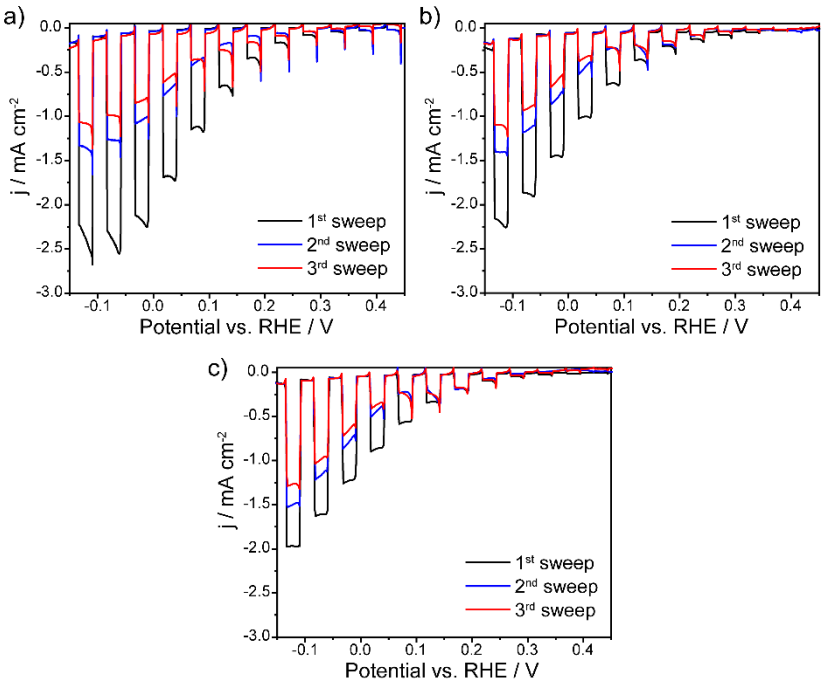

Fig. S10 Linear sweep voltammogram of the free-standing porous Cu_2O samples deposited at a) 5, b) 20 and c) 60 min deposition time.

LSV measurements were performed three times on each sample to investigate the chemical stability of the Cu_2O samples deposited at different times as was shown in Fig. S10. The photocurrent at 0 V vs. RHE for the 5 min deposited sample decreases significantly from -2.25 to -1 mA cm^{-2} while the photocurrent of the 20- and 60-min deposited sample reduces at a much slower rate. The thickest Cu_2O layer (60 min deposition time) has the lowest reduction of the photocurrent. This indicates that the thick bare Cu_2O film has higher photostability than the thin and more catalytic Cu_2O layer.

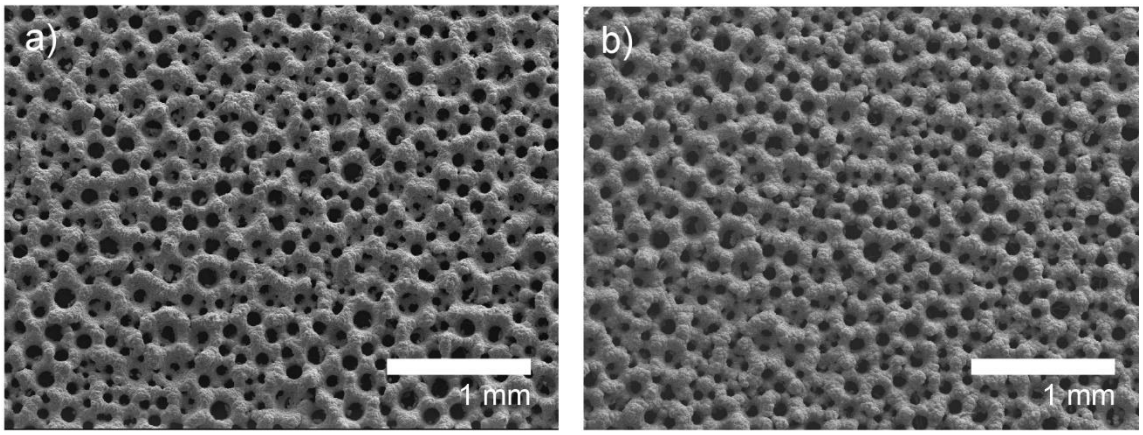

Fig. S11 Morphological images of two free-standing porous Cu_2O samples electrodeposited at -1.5 A cm^{-2} for 60 sec and reinforced with another electrodeposition process at -20 mA cm^{-2} for 120 min.

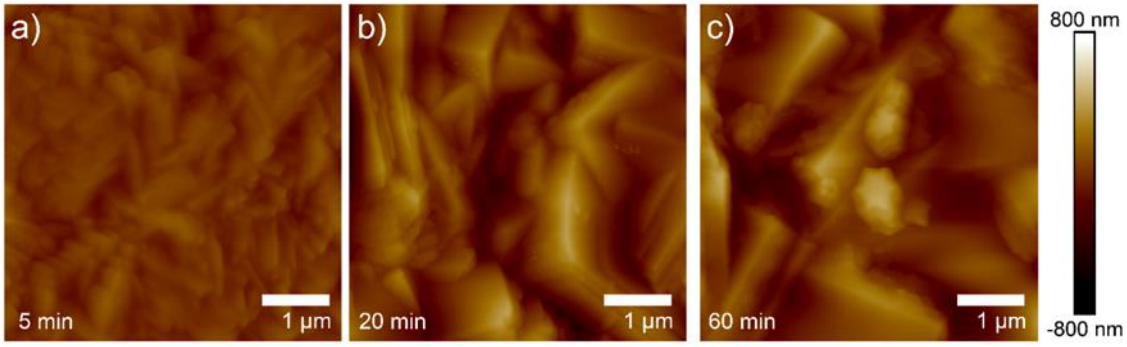

Fig. S12 AFM images of Cu_2O film deposited on free-standing porous Cu for a) 5 min, b) 20 min, and c) 60 min with surface roughness Rq of 53.2 nm, 149 nm, and 165 nm respectively.

Fig. S12a-c shows the morphology of the deposited Cu_2O film on the free-standing porous Cu framework. The samples of 5 min, 20 min, and 60 min have Rq values of 53.2, 149, and 165 nm respectively and the increase of the overall surface area from the Rq values was estimated to be 17 % (5 min), 35.7 % (20 min), and 41.3 % (60 min) from the geometric surface area by the NanoScope Analysis software.

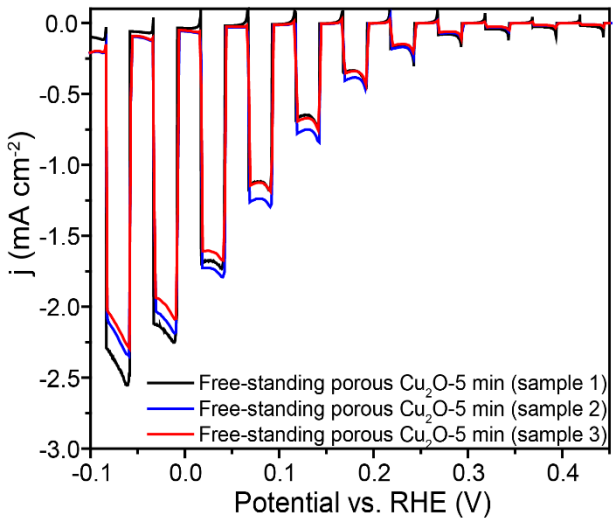

Fig. S13 Linear sweep voltammogram of electrodeposited Cu_2O film on three different free-standing porous Cu substrates synthesized with the same parameters (60-sec dendritic deposition and 120 min reinforcement procedure) in an aqueous electrolyte of 0.5 M Na_2SO_4 under chopped illumination.

The reproducibility of the free-standing porous Cu_2O samples electrodeposited with 5 min deposition for the PEC water splitting performance can be observed in Fig. S13. At the potential of 0 V vs. RHE, the current densities of the three samples are -2.2, -2.22, and -2.25 mA cm^{-2} for sample 3, sample 2, and sample 1, respectively. The small variation from the current densities shows that the samples can be easily reproduced.

Table S1. PEC water splitting performances of bare Cu_2O photocathodes reported in other publications.

Substrate	Structure	Fabrication method	Electrolyte	Photocurrent/ dark-current (at 0 V vs RHE)	Ref.
Flat Cu	Bare Cu_2O nanowires	Wet chemistry/ Thermal annealing	1 M Na_2SO_4	~-2.08 mA cm^{-2} / ~-0.3 mA cm^{-2}	[1]
Cu nanowires	Bare Cu_2O film	Thermal oxidation	1 M Na_2SO_4	~-0.5 mA cm^{-2} / Close to zero	[2]
FTO /Au	Bare Cu_2O film	Electrodeposition	1 M Na_2SO_4	~-2.4 mA cm^{-2} / Close to zero	[3]
FTO	Bare Cu_2O film	Electrodeposition	1 M Na_2SO_4 and 0.1 M formic acid	~-2.5 mA cm^{-2} / ~-0.25 mA cm^{-2}	[4]
FTO	Bare Cu_2O film	Electrodeposition	0.5 M Na_2SO_4	~-0.21 mA cm^{-2} / Close to zero	[5]
FTO	Bare Cu_2O	Electrodeposition	0.1 M Na_2SO_4	~-0.58 mA cm^{-2} /	[6]

				~-0.2 mA cm^{-2}	
Dendritic porous Cu	Bare Cu_2O film	Thermal oxidation	0.1 M Na_2SO_4	~-2.25 mA cm^{-2} / ~-1 mA cm^{-2}	[7]
Flat Cu	Bare Cu_2O film	Electrodeposition	0.5 M Na_2SO_4	~-1.25 mA cm^{-2} / Close to zero	This work
Free-standing porous Cu	Bare Cu_2O film	Electrodeposition	0.5 M Na_2SO_4	~-2.25 mA cm^{-2} / Close to zero	This work

References

1. Bai J, Li Y, Wang R, et al (2015) A novel 3D ZnO/Cu2O nanowire photocathode material with highly efficient photoelectrocatalytic performance. J Mater Chem A 3:22996–23002. https://doi.org/10.1039/c5ta07583a

2. Huang Q, Kang F, Liu H, et al (2013) Highly aligned Cu2O/CuO/TiO2 core/shell nanowire arrays as photocathodes for water photoelectrolysis. J Mater Chem A 1:2418–2425. https://doi.org/10.1039/c2ta00918h

3. Paracchino A, Laporte V, Sivula K, et al (2011) Highly active oxide photocathode for photoelectrochemical water reduction. Nat Mater 10:456–461. https://doi.org/10.1038/nmat3017

4. Kunturu PP, Huskens J (2019) Efficient Solar Water Splitting Photocathodes Comprising a Copper Oxide Heterostructure Protected by a Thin Carbon Layer. ACS Appl Energy Mater 2:7850–7860. https://doi.org/10.1021/acsaem.9b01290

5. Yang Y, Xu D, Wu Q, Diao P (2016) Cu2O/CuO bilayered composite as a high-efficiency photocathode for photoelectrochemical hydrogen evolution reaction. Sci Rep 6:1–13. https://doi.org/10.1038/srep35158

6. Wu H, Zheng Z, Toe CY, et al (2020) A pulse electrodeposited amorphous tunnel layer stabilises Cu2O for efficient photoelectrochemical water splitting under visible-light irradiation. J Mater Chem A 8:5638–5646. https://doi.org/10.1039/d0ta00629g

7. Ma X, Zhang J, Wang B, et al (2018) Hierarchical Cu2O foam/g-C3N4 photocathode for photoelectrochemical hydrogen production. Appl Surf Sci 427:907–916. https://doi.org/10.1016/j.apsusc.2017.09.075